

# Experimental investigation of the bubble distribution and chemical reactions induced by hydrodynamic cavitation inside a reactor - a preliminary study

Julius-Alexander Nöpel<sup>1\*</sup>, Patrick Zedler<sup>1</sup>, Manuel Deggelmann<sup>2</sup>, Patrick Braeutigam<sup>2</sup>, Jochen Fröhlich<sup>1</sup>, Frank Rüdiger<sup>1</sup>

<sup>1</sup> Technische Universität Dresden, Chair of Fluid Mechanics, Dresden, Germany

<sup>2</sup> Friedrich-Schiller Universität Jena, Institute for Technical Chemistry and Environmental Chemistry, Center for Energy and Environmental Chemistry (CEEC Jena), Jena, Germany

\* julius-alexander.noepel@tu-dresden.de

## Abstract

The paper deals with the experimental investigation of a cavitating free jet in water treatment. The focus of the study is to determine the correlations between global and local flow parameters and the efficiency of pollutant degradation as well as to establish an experimental procedure for further investigations in this sector. Therefore the areas of chemical oxidation of luminol induced by hydrodynamic cavitation in a reactor with two orifice geometries at different inlet pressures are identified. In addition, the bubble distribution of the cavitation jet in the reactor and the bubble sizes in a section next to the jet are determined by a laser light section method. Finally, this preliminary study links information of the chemical reactions with fluid mechanical properties. From the spatial characterization of chemiluminescence and the associated properties of the bubbles, conclusions can be drawn about the conditions at high degradation rates.

## 1 Introduction

The contamination of water by various substances, such as drugs, dyes, bacteria or viruses, receive increasing attention. Indeed, sensitive methods for detecting these have become available in recent years. The degradation of such water pollution can be achieved by hydrodynamic cavitation (e.g. Braeutigam et al. (2012)). Due to bubble collapses in the cavitation field, extremely high temperature, pressure and heating rates occur for fractions of seconds leading to a homolytic cleavage of water molecules creating short-living reactive species such as ( $\cdot\text{OH}$ ), ( $\cdot\text{H}$ ) and ( $\text{H}_2\text{O}_2$ ) (Braeutigam, 2016). These species contribute to degradation by oxidizing residues of the above substances, which is called advanced oxidation process (AOP).

## 2 Experimental setup

In this study the chemiluminescence of luminol in a cavitation reactor with an orifice forming a cavitating free jet in the reactor is investigated. The diameter of the orifice and the inlet pressure are varied in a flow of constant temperature at the inlet of the reactor.

The experimental setup (Fig.1a) comprises a tank, an inline plunger pump (variable speed, high pressure) with an electrical power of  $P = 3.5$  kW, maximum pressure of  $p_1 = 160$  bar, a maximum volume flow rate of  $\dot{V} = 10.3$  l/min, and the cavitation reactor. The cavitation reactor consists of a supply tube including an orifice and a glass cylinder serving as a reaction chamber (Fig. 1b). The length and diameter of the reactor and the thickness of the plate with the orifice are  $L = 71$  mm,  $D = 14.9$  mm,  $s = 2$  mm, respectively. Two different orifices were used in this study, one with diameter  $d = 1$  mm, the other with  $d = 1.7$  mm. The total volume of the system is  $V = 1.1$  liter. The flow is strongly accelerated when passing the orifice, resulting in a pressure drop down to vapor pressure and bubble growth, leading to a cavitating turbulent jet. The resulting cavitation bubbles in the reaction chamber are observable by optical methods. To reduce the influence of the curvature

of the glass cylinder, it is placed in a box of glycerine to increase the quality of high-speed recordings and shadowgraphy images. In case of chemiluminescence images, this box leads to diffuse reflections and had to be removed.

To ensure a constant temperature, a cooling system was installed. Two pressure manometers for  $p_1$  in the supply tube and  $p_2$  at the chamber outlet and a ultrasonic flow meter with an internal temperature sensor were used for monitoring the operating parameters (Fig. 1a). All components are entirely made of stainless steel.

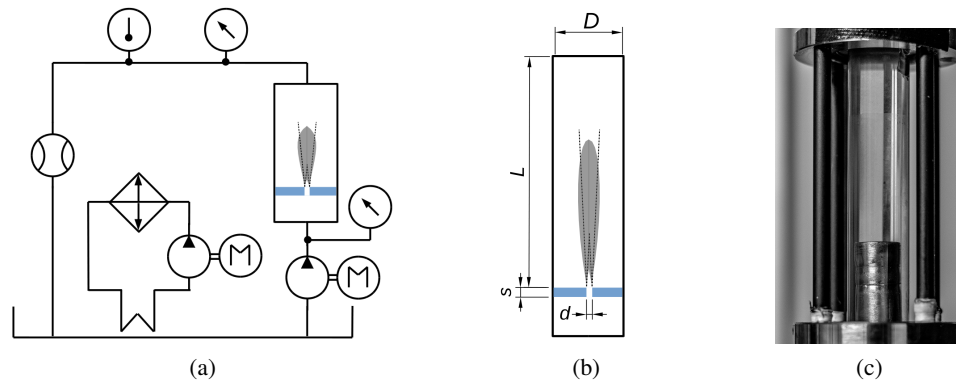


Figure 1: Cavitation test facility and reactor. a) hydraulic diagram, b) sketch with dimensions, c) photograph of the cavitation reactor with the glass cylinder and the stainless steel supply tube.

### 3 Chemiluminescence of luminol

The extreme thermodynamic states resulting from hydrodynamic cavitation lead to the homolytic cleavage of water, resulting in chemical reactions and chemiluminescence. The formation of reactive species, hydrogen radical ( $\cdot\text{H}$ ), hydrogen peroxid ( $\text{H}_2\text{O}_2$ ) and especially hydroxyl radicals ( $\cdot\text{OH}$ ), emerging by the induced chemical reactions cause AOP and reduction reactions at ambient temperature (Suslick et al., 1997). For the evaluation of the efficiency of degradation of organic substances obtained by hydrodynamic cavitation, information about the concentration of the resulting hydroxyl radicals are required. However, the highly reactive, non-selective hydroxyl radicals are short-living oxidants degrading on timescales of nanoseconds (Dorfmann and Adams, 1973). Therefore, it is difficult to detect them directly (Munter, 2001). Thus, a suitable marker for the spatial characterization of the hydroxyl radicals concentration is needed which is also quantifiable for measurements. For this purpose, chemiluminescence of luminol is often used (Finkbeiner et al., 2015). If cavitation occurs and if hydroxyl radicals are formed, the decomposition of luminol emits light, marking the place of chemical conversion in-situ which can then be detected by a camera. More precisely, the camera provides an integral value over a certain period of time and space.

For the measurement, 2 g/l luminol and 7.5 g/l sodium hydrogen carbonate were dissolved in distilled water under stirring, obtaining a solution with  $\text{pH} = 9.3$ . For image acquisition, the test stand was darkened to capture the emitted light with a digital single-lens reflex camera in long time exposure mode. Figure 2 shows the pictures of the spatial extent of chemiluminescence in the reactor chamber during an exposure time of  $t_e = 300$  s. A photo of the cavitation reactor is shown in Fig. 2g as a reference.

The images in Fig. 2a-f represent equally processed binary images to evaluate the extent, area and volume where chemiluminescence occurs. The white pixels represent regions of light emission. When converting to binary images, the information about the intensity distribution within the area is lost. For both orifice diameters, the area of white pixels increases as the pressure  $p_1$  is increased. When comparing the different orifice geometries at constant pressure  $p_1$ , a significantly larger expansion can be determined for  $d = 1.7$  mm, since the volume flow increases with the cross-sectional area of the orifice. The detected area of chemiluminescence at  $p_1 = 30$  bar with  $d = 1.7$  mm is almost twice as high and wide as for  $d = 1$  mm. The same is valid for  $p_1 = 20$  bar. With  $d = 1$  mm and  $p_1 = 10$  bar no light emission was recorded (Fig. 2f).

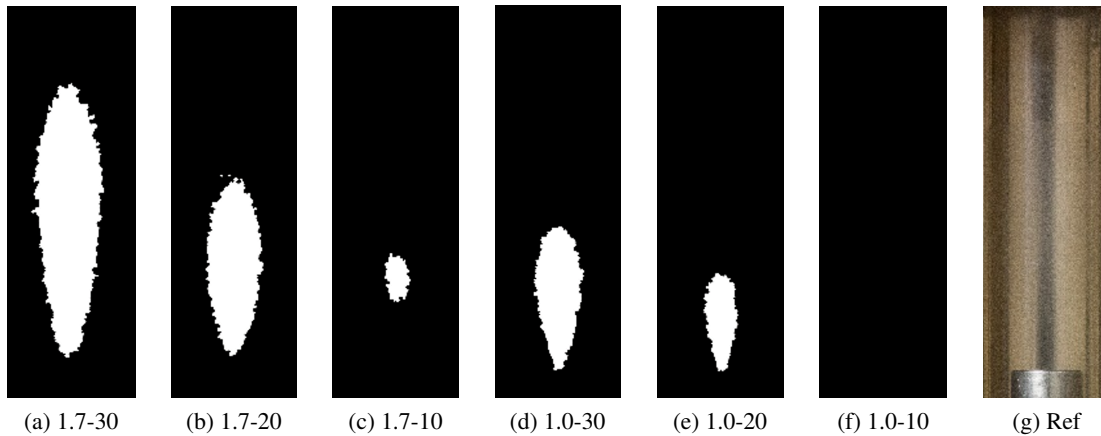


Figure 2: Spatial characterization of the chemiluminescence of luminol at  $T = 30\text{ }^{\circ}\text{C}$  for orifice  $d = 1.7\text{ mm}$  with a)  $p_1 = 30\text{ bar}$ , b)  $p_1 = 20\text{ bar}$ , c)  $p_1 = 10\text{ bar}$  and for orifice  $d = 1\text{ mm}$  d)  $p_1 = 30\text{ bar}$ , e)  $p_1 = 20\text{ bar}$ , f)  $p_1 = 10\text{ bar}$ . Geometrical reference g) reactor chamber.

In Fig. 3 the area of white pixels representing the expansion of light emission by chemiluminescence, normalized with the area of the reactor  $A_R$  is plotted as a function of  $p_1$ . Comparing both orifices at  $p_1 = 30\text{ bar}$ , the area with  $d = 1\text{ mm}$  is 26 percent of that with  $d = 1.7\text{ mm}$ . This result complies with the physical expectation that with a higher volume flow rate the degradation of luminol rises, so that the emission of light increases.

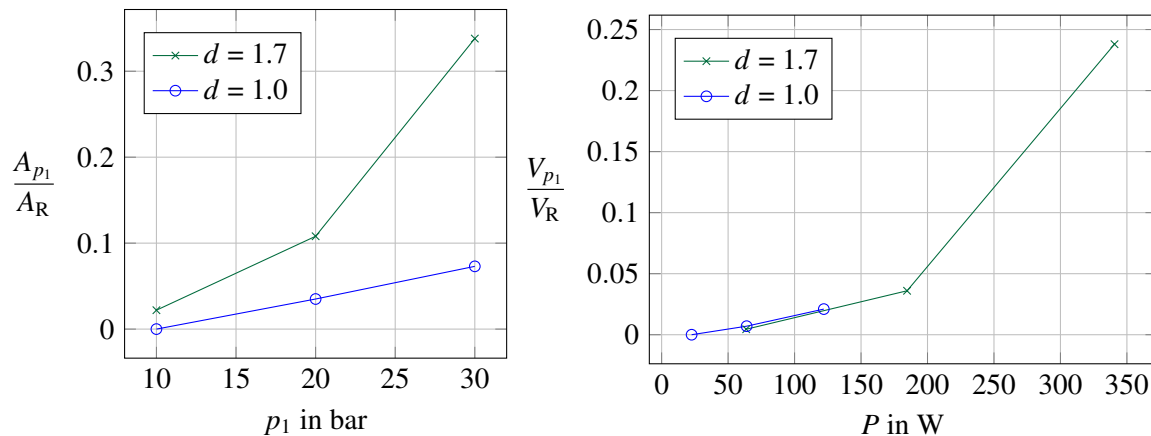


Figure 3: Comparison of the light emission by chemiluminescence of luminol caused by hydrodynamic cavitation for two orifices,  $d = 1.0\text{ mm}$  and  $d = 1.7\text{ mm}$ , at constant temperature of  $T = 30\text{ }^{\circ}\text{C}$ . Left: Area of chemiluminescence normalized by the central cutting plane area of the reactor as a function of inlet pressure  $p_1$ . Right: Volume of chemiluminescence normalized by the volume of the chamber of the reactor as a function of hydraulic power. Points connected by linear trend lines.

The hydraulic power of the flow is coupled via the energy balance to the rate of local evaporation and bubble growth and to the activation energy for chemical reaction, both volumetric quantities. The area of the emitted light can be converted into a volume, assuming axial symmetry. In Fig. 3, right, the volume normalized by the volume of the chamber of the reactor as a function of hydraulic power is shown. It can be seen that similar volume ratios occur at the same power, independent of the diameter of the orifice.

## 4 Bubble characteristics

The effect of chemiluminescence is caused by chemical reactions evoked by imploding bubbles. In a free jet the dominating cavitation phenomenon is vortex cavitation in the shear layer. With increasing distance from the orifice outlet, the kinetic energy of the free jet decreases and the local pressure increases, so that the probability of a bubble collapse increases as well.

In Fig. 2 the area of chemiluminescence is shown for different diameters of the orifice at different inlet pressure  $p_1$ . In the following the investigation focuses on the configuration with  $d = 1$  mm and  $p_1 = 20$  bar. For this case, it is necessary to estimate the time resolution which is needed to capture a sharp image. The orifice exit velocity can be calculated to  $w = 35$  m/s. The smallest length of one pixel is provided by the PCO 2000 camera, measuring  $l_{px} = 7.4$   $\mu\text{m}$  which can be used with a light sectioning method. The image scale to capture the whole chamber is set to  $m = 0.25$  and the minimal exposure time to  $t_b = 500$  ns. Hence, the maximal velocity for a sharp image can be calculated to  $w = 60$  m/s which is sufficiently resolved.

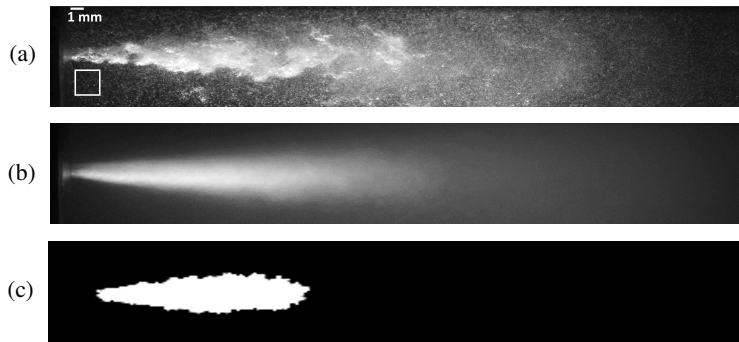


Figure 4: Comparison of the flow characteristics and the area of chemiluminescence for  $d = 1$  mm with  $p_1 = 20$  bar at  $T = 30$  °C, half the reactor is selected as image section from the exit of the orifice: a) Instantaneous image by laser light sectioning method. Exposure time of  $1/40000$  s. b) Visualization of the mean bubble distribution from arithmetic averaging of 800 instantaneous frames. c) Area of the emitted light by chemiluminescence.

Fig. 4a shows the instantaneous distribution of bubbles formed by hydrodynamic cavitation in the chamber of the reactor. At this operating point the Reynolds number is  $Re = 35,000$ . The image displays different levels of brightness which are related to a massive scattering of the light beam, coupled perpendicularly to the image recording plane. Bright areas are associated with high bubble concentration. In Fig. 4b the image displays the average of 800 instantaneous frames. Combining the information of Fig. 4a and 4b, it can be seen that areas of continuous cavitation clouds have dissolved up to  $x = 26 d$ .

Comparing the information of the fluid-mechanical properties of the cavitating free jet with the area of chemiluminescence, light emission in the range of  $x = 2 d$  to  $x = 15 d$  is recorded. It can be stated that in the area of the cavitation cloud, shortly after the nozzle exit until the end of the jet expansion and the decay of the cavitation cloud, the light emission can be detected over the recording period and, hence, marks the area of strong chemical reactions.

To determine the conditions during high chemical conversion, the properties of the cavitating free jet must be investigated. It is, therefore, important to determine the size of the bubbles in the region of chemiluminescence. An evaluation of the bubble diameters in the jet places extreme demands on optical measurement technology, since the imaging scale must be increased to  $m = 3$ . With the technical specifications of the PCO camera described above, an exposure time of less than  $t_b = 70$  ns is required, which could not be realised with the given system. However, it is possible to determine the bubble size in the recirculation area remote from the jet, since there the velocity is 10 times smaller. Fig. 5 shows the histogram of the averaged bubble number  $N$  at several classes of the bubble diameter  $d_b$  for different values of  $p_1$ , averaged over 800 instantaneous individual images. The reference area for evaluation is shown in Fig. 4a by means of a white frame. It can be seen that at different pressures  $p_1$  different bubble size distributions occur in the recirculation area. The smaller the inlet pressure  $p_1$ , the smaller the number of small bubbles.

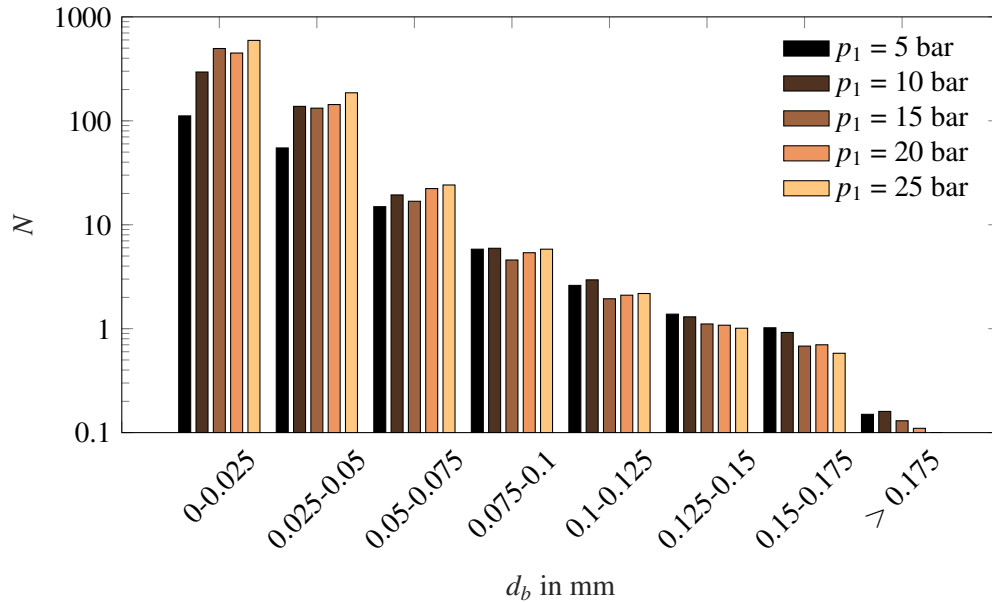


Figure 5: Histogram of the averaged bubble number  $N$  for several classes of bubble diameter  $d_b$  with different values of  $p_1$  obtained with the  $d = 1$  mm orifice (800 frames, analysed on a  $4 \times 4$  mm area near to the cavitating jet, cf. white frame in Figure 4a).

Furthermore, it becomes clear that at high  $p_1$  rather small bubbles are detectable. This corresponds to the assumed physics that for higher pressure  $p_1$ , more bubbles with a smaller diameter are formed. Due to the high concentration of gas bubbles, implosion can be dampened, which is equivalent to a degassing process. Finally, the uncertainty of the bubble size determination must be pointed out. It increases with decreasing diameter of the bubble since the smallest specific diameter is resolved by only two pixels. The large number of individual images evaluated provides sufficient statistical certainty.

## 5 Concluding Remarks

The preliminary study presented here shows the dependence of the chemiluminescence of luminol on the inlet pressure and the orifice geometry. It was found, that similar volumes of chemiluminescence are generated at the same hydraulic power, independent of the cross-sectional area of the orifice. Intense chemical reactions occur at locations with high bubble concentration, and an increasing inlet pressure results in an increasing concentration of bubbles and an increase in the area of emitted light. Higher degradation rates were achieved with the larger orifice diameter in a shorter time.

Future activities will aim at determining the conditions for optimal degradation rates at which the energy employed is used efficiently. The objective long term is to provide validation data for numerical models predicting substance degradation rates.

## Acknowledgements

This work was supported by the federal ministry for economic affairs and energy (BMWi) by a resolution of the German Bundestag (16KN073422, ZF4050703RH6).

## References

Braeutigam P (2016) Degradation of Organic Micropollutants by Hydrodynamic and/or Acoustic Cavitation. *Handbook of Ultrasonics and Sonochemistry* pages 761–783

Braeutigam P et al. (2012) Degradation of carbamazepine in environmentally relevant concentrations in water by Hydrodynamic-Acoustic-Cavitation (HAC).. *Chemical Engineering Journal* 46:2469–2477

Dorfmann L and Adams G (1973) Reactivity of the hydroxyl radical in aqueous solutions. *National Standard Reference Data System*

Finkbeiner P et al. (2015) Sonoelectrochemical degradation of the anti-inflammatory drug diclofenac in water. *Chemical Engineering Journal* pages 214–222

Munter R (2001) Advanced oxidation processes: current status and prospects. *Proc Estonian Acad Sci Chem* 50:59–80

Suslick KS, Mdleleni MM, and Ries JT (1997) Chemistry induced by hydrodynamic cavitation. *Journal of the American Chemical Society* 119:9303–9304